Journal of Pharmaceutical Innovation
https://doi.org/10.1007/s12247-022-09642-0

ORIGINAL ARTICLE

Rheological and Structural Study of Solid Lipid Microstructures Stabilized within a Lamellar Gel Network

Mohamed Kouider Amar[1,2,3,4] · Soufiane Rahal[4] · Maamar Laidi[1,2,4] · Redha Rebhi[4] · Mohamed Hentabli[1,2,3,4] · Salah Hanini[1,2] · Mabrouk Hamadache[1,2]

Accepted: 22 March 2022
© The Author(s), under exclusive licence to Springer Science+Business Media, LLC, part of Springer Nature 2022

Abstract

Purpose This study aimed to investigate the influence of different ratios and amounts of cetyl and stearyl fatty alcohols in interaction with cetyl palmitate fatty acid ester as they are responsible for the rheological and microstructural modifications in the SLMs.

Methods SLMs were prepared as ternary systems in the absence of an oil phase; Tween 80 was selected as nonionic surfactant that was blended with the fatty amphiphiles forming the lipid phase, and ultra-purified water constituted the aqueous phase; the hot emulsification and high shear homogenization methods were used to produce the SLMs, and central composite face design was used to evaluate and model the SLMs particles size, polydispersity, and rheological parameters.

Results The formulated SLMs have an average particle size ranging from 18.4 to 59.4 µm which showed that the lipids' ratio and amount have affected significantly ($p < 0.05$) the rheological and microscopic parameters, and the optimization led to lipid combination of SA/CA/CP/0.41:0.41:0.18 with a consistent structure and shear thinning behavior. The drug-loaded SLMs have a sustained release profile up to 12 h with a release rate ranged from 1.6 to 2.6 mg/h for 12% and 9% lipids content formulations.

Conclusion The rheological and microstructural behaviors of the studied SLMs are strongly related with the swelling capacity of the formed gel network, while their ratios, amounts, and storage time controlled the structure. The findings in this study may provide further insights of SLMs rheological and structural behaviors in different dispersion mixtures.

Keywords Formulation · Solid lipid microstructures · Central composite face design · Stability · Lamellar gel network

Introduction

Pharmaceutical and cosmetic creams are widely studied due to their complex structures that extend from a simple water and oil mixture to a structured semisolid system in which emulsifiers and co-emulsifiers are employed as stabilizers and vehicles for the pharmaceutical active ingredients (API) and the cosmetic substances. In the absence of an oil phase surfactant–fatty amphiphiles–water mixture is designated as ternary system that can assume the influence

✉ Mohamed Kouider Amar
kouideramar.mohamed@univ-medea.dz

Soufiane Rahal
rahalsoufiane@yahoo.fr

Maamar Laidi
maamarw@yahoo.fr

Redha Rebhi
redha.rebhi@univ-medea.dz

Mohamed Hentabli
Hentabli.mohamed@univ-medea.dz

Salah Hanini
hanini.salah@univ-medea.dz

Mabrouk Hamadache
hamdeche.mabrouk@univ-medea.dz

[1] Biomaterials and Transport Phenomena Laboratory (LBMPT), University Yahia Fares of Medea, 26000 Medea, Algeria

[2] Department of Process Engineering, Institute of Technology, University Dr Yahia Fares of Medea, Medea, 26000 Medea, Algeria

[3] Laboratory of Quality Control, Physico-Chemical Department, SAIDAL of Medea, 26000 Medea, Algeria

[4] Faculty of Technology, University Dr Yahia Fares of Medea, Medea, 26000 Medea, Algeria

Published online: 12 May 2022

of the emulsion continuous phase [1]; these mixed emulsifiers are usually blended to form the dispersed phase in the free bulk water; in excess of mixed emulsifiers, the emulsion structural and rheological behaviors are related to the formed viscoelastic lamellar crystalline structure according to the gel network theory [2].

The gel network theory is an explanation to the self-assembly of emulsifiers such as fatty alcohols and surfactants that combine in the continuous phase of an O/W cream and its stability increases by the intervention of a strength gel structure; the latter is being a multiphase structure that exhibits a viscoelastic and shear-thinning rheological behaviors relatively to the combination between the used fatty amphiphiles and their resultant swelling capacity [3]. Eccleston has developed this theory as a result for his studies on emulsions and ternary systems [1]; these systems form at least three phases: (i) hydrophilic gel phase composed of bilayers of surfactant, fatty amphiphiles, and interlamellar fixed water, (ii) lipophilic gel phase formed by the excess of fatty amphiphiles, and (iii) the bulk water phase that is in equilibrium with the interlamellar fixed water. The swelling characteristic of the lamellar region in the system is caused by the electrostatic repulsions or hydration of the polyoxyethylene chains respectively for ionic and nonionic nature of the surfactant [4–6]; the lamellar gel network phase is more thicken and more swelled which trap the oily droplets and prevent their coalescence [7–9].

Solid lipid microparticles (SLMs) having an average particles size over 1 μm can be formulated by mixing fatty alcohols and fatty acid esters using high energy shear homogenization technique that can nanometrically rescaled to obtain the solid lipid nanoparticles (SLNs); SLMs are produced by the simple heating and cooling emulsification method and their importance lie in their raise efficiency for different administration routes including topical application [10, 11].

According to previous studies, solid lipid micro/nanoparticle constituents are equivalent and both are used as drug carrier; their main differences are in the particle size and administration route; the SLMs' particle size is higher than the SLNs; however, the SLMs can be suitable for higher drug loading and an efficient entrapment [12]. In the pharmaceutical field, the vehicle particles size have not as much importance as the administration route by which the API is delivered; in addition, the toxicity that can be induced is more worrisome and an important factor for the selecting [13]; in the other hand, SLMs' rheological and structural properties are still by far less studied, as yet their less industrial usability; SLMs give more advantageous industrial scaling-up that the production of these dispersion systems is simple, less expensive, and time and energy gaining compared to the SLNs that are produced by the high-pressure homogenization technique [14].

Topical pharmaceutical dosage forms and cosmetic ingredient deliverance by semisolid forms need a sufficient high viscosity, consistency, and a thixotropic flow behavior to ensure a good adherence to the skin [15]; rheologically, liquid like SLNs are not suitable and less beneficial for topical administration route due to their low consistency and conditioning difficulties; these SLNs have to be passed to a second-step process in which they are incorporated in a secondary semisolid mixture like ointments, gels, or creams to achieve the desired consistency for topical use and to guarantee a longer contact with the administration site; this long process can be avoided in the case of SLMs [16].

Cetyl palmitate fatty acid ester has been widely used in pharmaceutical cream formulations in combination with fatty alcohols, with the aim of improving a controlled drug release and an enhanced drug penetration into the skin [17]; in addition, these fatty amphiphiles have been also used to control the consistency and stability of the semisolid formulations due to their "bodying action" properties [18].

Furthermore, fatty amphiphiles are a suitable medium to dissolve or entrap an active principle ingredient (API) that has a highly lipophilic nature and a poor solubility in aqueous and/or organic solvents; this lipid drug delivery system is highlighted as important in topical dosage forms such as lipid emulsions that are the most industrially used drug carrier; in contrast, there are few solid lipid microparticles (SLMs) drug delivery systems and commercialized products [19]; these type of lipid-based formulations are more effective compared to lipid emulsions in terms of drug leakage, particles growth, and stability during storage; in addition to the possibility for a controlled and targeting drug release, the SLMs can be an alternative form to improve the safety and increase the function durability of an active substance that is protected by the biocompatible and physicochemical stable lipid layers [20].

The investigations that have been made in order to optimize the ratio of fatty alcohols with different hydrocarbon chain lengths are ended by different results and theoretical conclusions [21]; for this concern, design of experiments (DoE) method can serve the necessity for a physical and coherent interpretation by using the response surface methodology (RSM) that showed an increment interest in different fields including the pharmaceutical industry and showed the efficiency in studying the rheological and structural behaviors of different materials [22–25].

RSM is a troubleshooting method that was used in this study to analyze and improve the rheological and structural properties of SLM-based formulations stabilized within a lamellar gel network. RSM uses a set of mathematical and statistical approaches in order to optimize complex processes which are dependent in all cases on more than one factor which make the interpretation of the results more complicated, the principal factors influencing the performance of

the process are selected and named inputs, and their potential of influence is determined from the response resulted from the measured parameter(s); these responses are named outputs, and then, a statistical relationship between the variables and responses is provided and represented by mathematical models that deduce the predictions and give a large spectrum of approximation; the methodology can be helpful in the design and the optimization of the SLMs form, function, and stability [26, 27].

The objective of this work is to study and optimize three lipid ratios and amounts of stearyl alcohol (SA), cetyl alcohol (CA), and cetyl palmitate (CP) in semisolid SLM formulations using the microstructural, rheological, and statistical methods to improve their stability and applicability in the pharmaceutical and cosmetic industries.

Materials and Methods

Materials

Stearyl alcohol EP ($C_{18}H_{38}O$, T_m: 58.6 °C) was purchased from Transmare Chemie NV (Belgium), cetyl alcohol EP ($C_{16}H_{34}O$, T_m: 50.9 °C) was purchased from Industria Chimica Panzeri srl (Italy), cetyl palmitate 95 EP ($C_{32}H_{64}O_2$, T_m: 53.2 °C) was purchased from Axo Pharma (Belgium), polysorbate 80 EP ($C_{64}H_{124}O_{26}$) was purchased from Mosselman Oleochimicals (Belgium), purified and filtered (0,22 µm) water was purchased from Milli-Q® system (0.055µS/cm at 26 °C, TOC: 3 ppb), terbinafine HCl EP (100.2%) was purchased from Shandong Boyuan Pharmaceutical Co., Ltd., and the other chemicals were of analytical reagents grade.

Methods

Preparation of the Samples

The formulations were prepared in a random order according to the given CCF design in Table 1 in which some of the proposed levels were modified as illustrated by the coded values. A fixed equal amount (1.2 wt) of fatty alcohols was added to their limits compared to the cetyl palmitate to enhance the stability of the preparations based on a recently made study for ternary systems containing the same fatty alcohols and Tween 60 as nonionic [21].

The purpose of using weight units was to study the effect of constituent's ratios in the mixture as well as their total amount; thus, at least three batches of 60 g for each experience were formulated by the hot emulsification method whereby ternary systems are usually formulated proceeding as follow:

Firstly, the oil phase contained the designed amounts of SA/CA/CP and T80 mixture and an aqueous phase which contained PW were heated oily and aqueous phases at temperature of 75 ± 5 °C which is above the highest component melting point, a hand stir allowed a complete melting and homogeneity of the oily phase, then the oily mixture was added dropwise to the aqueous phase that was maintained under magnetic stirring for 2 more min at the same temperature, after this step, a vigorous stirring was applied to the

Table 1 Central composite faced design with coded levels and the corresponding weight compositions

Name/run order	SA	CA	CP	SA (wt)	CA (wt)	CP (wt)	PW (wt)	T80 (wt)
FN01/08	−1	−1	−1	2.2	2.2	1.0	90.0	2.0
FN02/06	+1	−1	−1	5.2	2.2	1.0	90.0	2.0
FN03/16	−1	+1	−1	2.2	5.2	1.0	90.0	2.0
FN04/02	+1	+1	−1	5.2	5.2	1.0	90.0	2.0
FN05/04	−1	−1	+1	2.2	2.2	4.0	90.0	2.0
FN06/14	+1	−1	+1	5.2	2.2	4.0	90.0	2.0
FN07/03	−1	+1	+1	2.2	5.2	4.0	90.0	2.0
FN08/12	+1	+1	+1	5.2	5.2	4.0	90.0	2.0
FN09/15	−1	0	−0.333	2.2	3.7	2.0	90.0	2.0
FN10/11	+1	0	−0.333	5.2	3.7	2.0	90.0	2.0
FN11/10	0	−1	−0.333	3.7	2.2	2.0	90.0	2.0
FN12/01	0	1	−0.333	3.7	5.2	2.0	90.0	2.0
FN13/09	0	0	−1	3.7	3.7	1.0	90.0	2.0
FN14/13	0	0	0.8	3.7	3.7	3.7	90.0	2.0
FN15*/07	0	0	0	3.7	3.7	2.5	90.0	2.0
FN16*/05	0	0	0	3.7	3.7	2.5	90.0	2.0
FN17*/17	0	0	0	3.7	3.7	2.5	90.0	2.0

SA stearyl alcohol, *CA* cetyl alcohol, *CP* cetyl palmitate, *PW* purified water, *T80* Tween 80

*Centre points

total mixture, and the high shear T25 digital ULTRA-TURRAX® homogenizer at 16.000 rpm was utilized mostly not more than 1 min at room temperature in which the creamy aspect appeared and no further more agitation was applied.

Finally, the preparations were left to cool down at room temperature and preserved in adequate containers with an orifice to facilitate their upcoming use.

Macroscopic and Microscopic Analysis

In order to control the homogeneity and the consistency or visual instabilities, the samples were examined visually during more than 3 months of storage at 25 °C.

Optical microscope (Olympus, Japan) was used to analyze the microstructure of the prepared ternary systems by gently applying a thin layer from the cooled down semisolid preparation and spread out on the slide of the microscope.

The microscopic examination was carried out after at least 4 h (T0) of cooling down to room temperature that the system had the consistent semisolid appearance, and after 3 months, the analysis was repeated in the same apparatus by using a fixed digital camera with a sufficiently high resolution. The images were calibrated in different magnifications, and at least 300 particles were examined using the image processing software ImageJ from (US National Institutes of Health).

Particles that showed an acceptable spherical form have been chosen to the examination of the arithmetical mean diameter (d_m) and its corresponding polydispersity (D) and Sauter mean diameter ($d_{3,2}$) that were calculated by the following formulas [28]:

$$d_m(\mu\mathrm{m}) = \sum_{i=1}^{n} f_1 \cdot d_1 \tag{1}$$

$$\mathrm{d_{3,2}(\mu m)} = \sum_{1}^{n} \mathrm{f_i \cdot d_i^{\,3}} \Big/ \sum_{1}^{n} \mathrm{f_i \cdot d_i^{\,2}} \tag{2}$$

$$D\,(\%) = s/d_m \cdot 100 \tag{3}$$

where f_i and d_i are the frequency and its central diameter, respectively, and s is the standard deviation of the particles size distribution.

Rheological Measurements

Flow and Thixotropic Behaviors

All the rheological measurements were carried out in triplicates and for periods of 1 month steps in order to allow the samples to recover and to follow the rheological changes occurred during storage time. The analysis was done in the same experimental conditions using a controlled shear rate Bohlin Visco88 (Malvern Instruments Ltd., UK) rotational viscometer, equipped with a cup and bob (coaxial cylinders) geometry. Two appropriated cylinders were used to perform the rheological tests with inners (25 mm)/(14 mm) and outers (27.5 mm)/(15.4 mm) diameters, respectively.

The samples have been poured carefully into the cup and allowed to rest for at least 10 min under a constant laboratory temperature of 24 °C ± 0.2 °C before the measurement; in this step, the limit of the torque controlled the maximum shear rate to be used to decide the sweep range; flow curves were obtained over a shear rate sweep up to $2004\mathrm{s}^{-1}$.

After several model comparisons, the curves obtained from the shear stress versus shear rate are described by the following Ostwald de Waele relationship (power law model) Eq. (5).

$$\tau = K \cdot \dot{\gamma}^{n} \tag{4}$$

where τ (Pa) is the shear stress and $\dot{\gamma}$ (s^{-1}) is the shear rate; K and n are the consistency coefficient and the power law index, respectively, with $(0 < n < 1)$.

The yield stress τ_0(Pa) is also a parameter that provides information on the viscoelasticity of the non-Newtonian fluids [29], that at a critical shear rate or strain, the stress is released which refers to an end of the linear viscoelastic region (LVE) and the beginning of the non-linear viscous behavior; this rheological parameter is directly related to the stability of the structure, and it can be determined from the flow curves by the Casson's model Eq. (6) [30].

$$\tau^{0.5} = \tau_0^{0.5} + (\mu \cdot \dot{\gamma})^{0.5} \tag{5}$$

The choice of these parameters was based on the shear rate range, and both R^2 and the adjusted R^2 of the fit, which are highly significant to be modeled.

The thixotropic behavior was studied in the second month stored formulations and was evaluated firstly by recording the stress response to the imposed shear rate sweep upward to 219 s^{-1} and downward ramp to 16 s^{-1} and the hysteresis loop curves generated by this test were integrated using OriginPro data analyzer in which the polygon absolute area was obtained.

Transient Shear Flow and Time Dependency

The time-dependent stress decay was determined by monitoring the stress over time by three successive ($\Delta t = 0$) shear rate steps as represented schematically in Fig. 1.

The first shear rate step was applied for 60 s at the lowest shear rate 16 s^{-1} provided by the viscometer, and the second and third steps were monitored for 120 s at shear rates of

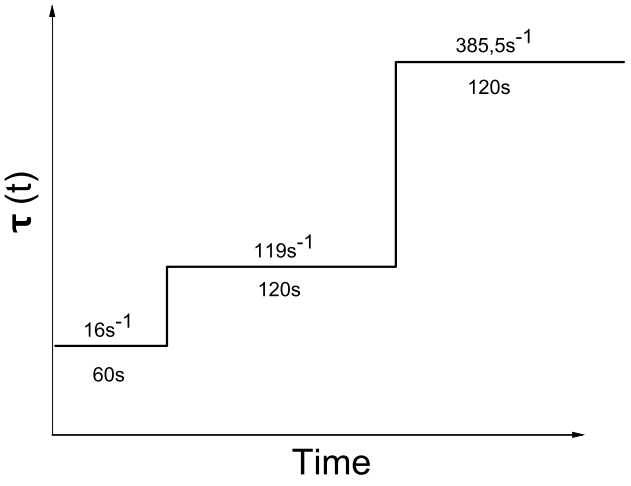


Fig. 1 Schematic representation of multiple shear rate steps and durations applied to carry out the transient shear flow experiments

119 s^{-1} and 385.5 s^{-1} which can simulate the hand rubbing when applying topical semisolid forms, and the duration of these latter two steps was fixed at 120 s that was sufficient to evaluate and quantify the structural breakdown using modified Weltmann model with two parameters Eq. (9) [31]; this model provide information on the extent of thixotropy (B) and the maximal reached shear stress (A), this model was widely employed to study the thixotropic behavior of non-Newtonian pseudo-plastic fluids, and it is dependent of the shearing time [32].

$$\tau = A - B \cdot [log(t/tm)] \quad (6)$$

where τ is the stress (Pa), A is the intercept with the stress axis (Pa), B is structural breakdown (Pa), t is time (s), and t_m (s) is a fixed time parameter at the maximal stress that was observed.

Data fitting was applied for times after a maximal stress was observed ($t > t_m$).

Experimental Design and Statistical Analysis

Central composite face (CCF) design is a cubical design that each factor has three levels (−1, 0, +1) corresponding to (min, center, max), and the axial points are placed on the center face of the cube (α = 1); three center points were designed to characterize the experimental pure error and reproducibility, and this type of experimental design proved an efficiency to study and optimize the pharmaceutical application of solid lipid microparticles [17].

The second-order polynomial model Eq. (7) was firstly used to fit the collected data obtained from the microscopic and rheological examinations, and the approximation by multiple linear regressions (MLR) method was applied to determine the influence of the three independent variables presented in Table 1, while the non-significant ($p < 0.05$) terms were removed from the model, and transformation was applied if necessary using Box-Cox tool to compute the best model transformation available to better statistics expression. The design of experiment software (Modde 6.0) (Umetrics, Sweden) has been used to illustrate the statistical interpretation of the microscopic and rheological parameters that were used as responses to the previously mentioned three factors (SA/CA/CP) that have a minimum and maximum levels, respectively, for 2.2/2.2/1 and 5.2/5.2/4; the software also was used to optimize the fatty amphiphiles ratio that can produce the best possible combination leading to longer stability.

$$\hat{Y}_1 = \beta_0 + \sum_{i=1}^{3} \beta_i x_i + \sum_{i=1}^{3} \beta_{ii} x_i^2 + \sum_{i=0}^{2} \sum_{i<j}^{3} \beta_{ij} x_i x_j \quad (7)$$

where $\hat{Y}_i$ is the response function, β_0 is a constant, β_i, β_{ij} and β_{ii} are the linear, interaction, and quadratic coefficients respectively, while x_i and x_j are the factors coded levels.

Terbinafine-HCl-Loaded Solid Lipid Microparticles

In order to verify the application of the developed models in different circumstances, terbinafine hydrochloride (TBH) was chosen as a drug model based on its solubility in the used surfactant [33] and its common use with the studied fatty amphiphiles [34]. TBH was loaded into the optimized SLMs ratio at three different lipids which have total amount of 6%, 9%, and 12% (wt), respectively; the incorporation was done to the melted lipid mixture while the conditions were maintained the same as previously detailed in the preparation of the samples part; the three formulations named TBH-SLM-6, TBH-SLM-9, and TBH-SLM-12 were investigated using the same microscopic and rheological methods.

Percentage Drug Content

Dispersion of 2 g from the SLMs in 10 ml of methanol is vigorously mixed, and after then, a cooling centrifugation at 2000 rpm and 4 °C for 30 min was applied to separate the supernatant that was filtered after then (0.45 µm membrane filter) and diluted (1/100) to obtain an equivalent drug concentration of 0.02 mg/ml. The preparation was analyzed by UV spectrophotometer (Perkin Elmer Lambda 25) analysis at λ_{max} 283.5 nm after a scan of wavelengths in the UV domain, a standard solution having the same concentration was prepared as a reference, and methanol was used as the blank.

In Vitro Drug release and Permeation Studies

The in vitro release was studied using a modified Franz cell with a surface area of 3.9 cm^2 and the temperature of the 100 ml receptor compartment was maintained at 32 ± 0.5 °C, and the latter was agitated at 50 rpm. Cellulose acetate was used as the diffusion barrier which on top is spread with 1 g of the sample and placed between the two compartments (donor and receptor). The donor was filled with 5 ml phosphate buffer pH 5.8 [34] that is used as the receptor medium. Five milliliters from the buffer containing the released drug was withdrawn each hour and replaced by an equivalent fresh buffer volume. Samples were collected for 12 h and analyzed using UV spectrophotometer (Perkin Elmer Lambda 25) at λ_{max} 222.7 after a scan of the wavelengths in the UV domain.

The cumulative drug release was modeled by the Higuchi model Eq. (8) [35]:

$$Q\ (\%) = K_H \cdot t^{1/2} \tag{8}$$

K_H: Higuchi's model release rate constant.

The permeation through the cell area was calculated using Eq. (9) [36]:

$$J_{ss}\ (\mu g/cm^2/h) = dQ/(A \cdot dt) \tag{9}$$

where $\frac{dQ}{dt}$ is the slope of the steady-state drug release profile and A is the area of the diffusion (cm^2).

Results

Formulation of the SLMs

In this work, SA, CA, and CP were used as the core lipids for the preparation of the SLMs; these excipients are reported inactive and safe and included in the Food and Drug Administration (FDA) Database and in the Canadian List of Acceptable Non-medicinal Ingredients; the levels of the weights reported in this study were chosen based on the usual ranges employed in the cosmetic and pharmaceutical topical formulations [37–39]. The surfactant was used in excess of that required to stabilize the formulations, which is employed to lower the surface tension and to solubilize the particles aggregates [8, 40] and the contribution in formation of the gel network structure [4].

Sufficient time has been taken to ensure that the ingredients have fully melted before the emulsification step which helps in homogeneous dispersion and avoids formation of large lipid particles in the mixtures. As noticed during the preparation of the SLMs, formulations with high amount of lipids showed rapid formation of the creaminess compared to other formulations; however, a misuse of the homogenizer can lead to serious problems like phases separation; in the formulation of the SLMs, homogenization must cover all the area of the mixture when the temperature is above the highest component melting point.

Macroscopically, all the resultant formulations have a white creamy appearance that presented firstly a liquid-like flow before they cooled down to room temperature, and different consistencies were remarkable that increased relatively in time until a final homogeneous semisolid appearance was wind up. There is an apparent slight visual change in the consistencies in the case of FN01 and FN05, for example, after they were subjected to stress (rheological tests), and in contrast, no phase separation was observed during the examination time when the formulations were stored at room temperature in the absence of stress.

Microscopic Results

The two times (T0 and T3) corresponding to the 4th h and the 3rd month from the first preparation were selected for the statistical evaluation of the microscopic parameters (Figs. 2, 3 and 4), because these complex systems can take several weeks to reach the equilibrium state [41].

The statistical results were expressed by the quadratic and second order polynomial models as responses for the T0 and T3 analysis. The statistically significant terms ($p < 0.05$) were kept and those with p-values > 0.05 were removed from the models; hence, the coefficient of determination R^2 ranging from 0.982 to 0.997 was enhanced, and similarly for the adjusted coefficients of determination R^2_{adj} that were ranged from 0.976 to 0.995, indicating that the models have highly fitted the data, and the selected terms constituting the models presented no significant lack of fit ($p > 0.05$) when analyzed by ANOVA test.

The Sauter (d3,2) mean diameter model for T0 and T3 were half powered; $\left(\widehat{Y}' = \widehat{Y}^{1/2}\right)$ thus, the predicted responses should be double powered $\left(\widehat{Y}'_2 = \widehat{Y}\right)$ to obtain the true values; this operation allowed an increment in both R^2 and R^2_{adj}; consequently, the linearization of the observed versus predicted values and the Q^2 which represent the model predictive goodness were enhanced, while model's validity is always higher than 0.25 which is the lower limit to an acceptable model.

Modeling the Microscopic Parameters

The following models represent respectively the responses related to the three factors.

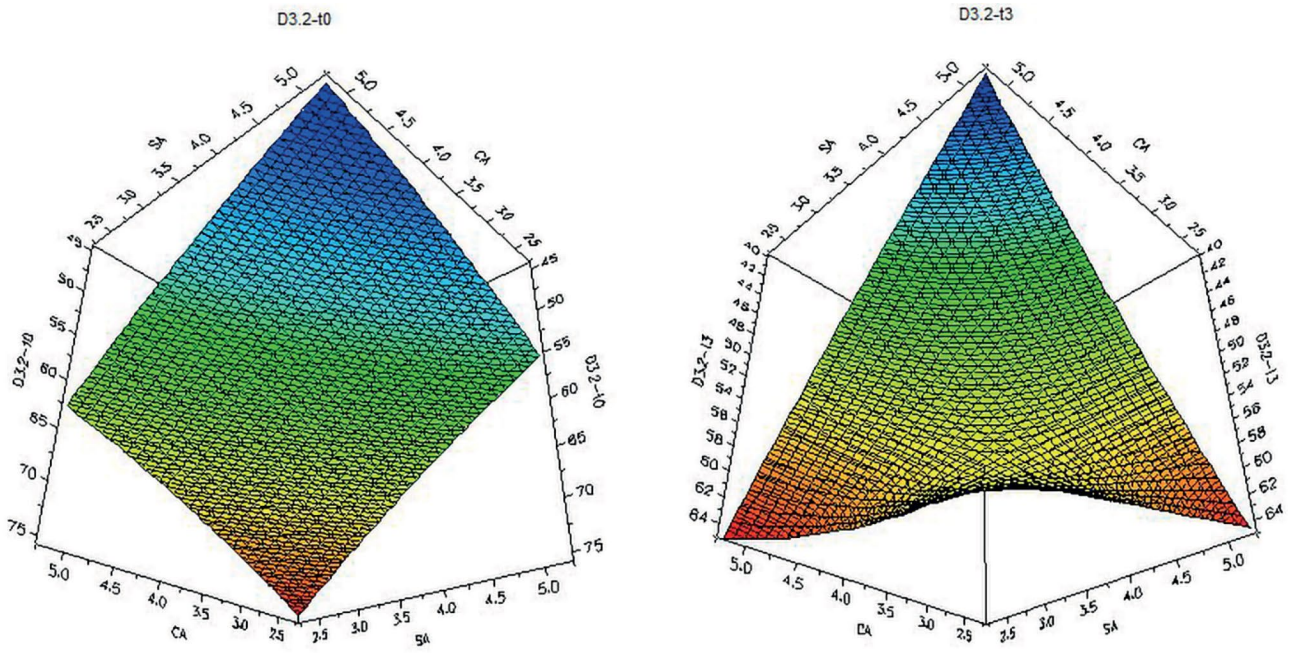


Fig. 2 Response surface plot for factors' effect on SMD between T0 and T3 analysis, respectively, from left to right

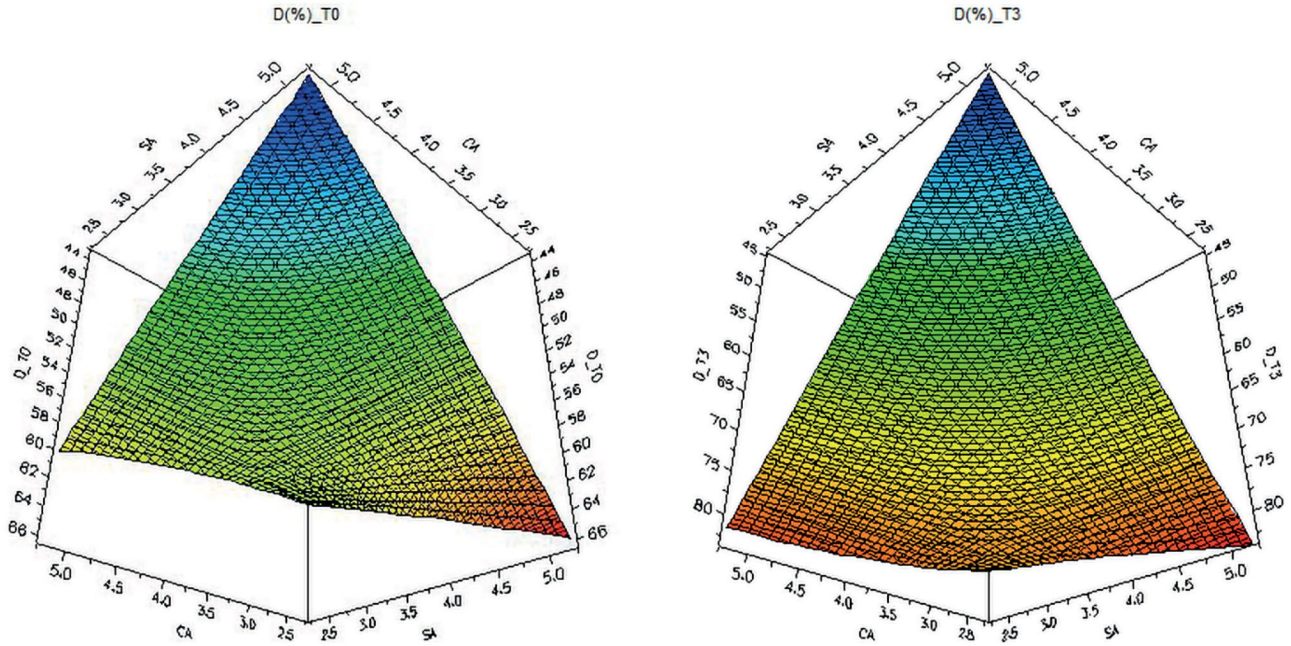


Fig. 3 Response surface plot of the factors' (with centered level of CP) effect on polydispersity, from left to right in T0 and T3 examination periods

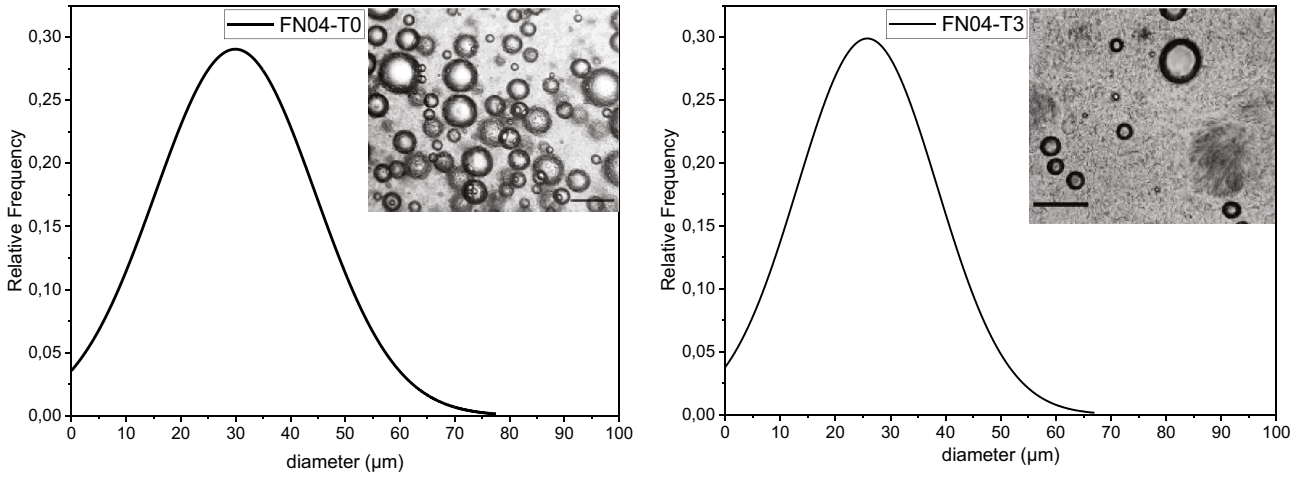


Fig. 4 Optical micrographs of the 4th formulation showing a typical shape of particles and their normal distribution that illustrates the reduction in size between T0 and T3 with more interparticular spacing (scale bare: 100 µm)

The arithmetical mean diameter response for T0 and T3 times is modeled by the following $\widehat{Y}_1$ and $\widehat{Y}_2$ responses, respectively:

$$\widehat{Y}_1(\mu\text{m}) = 36.06 - 4.85x_1 - 2.26x_2 + 7.42x_3 + 3.23x_1x_2 - 4.11x_1x_3 - 1.77x_2x_3 \quad (10)$$

$$\widehat{Y}_2(\mu\text{m}) = 28.16 - 0.58x_1 + 1.71x_2 + 4.85x_3 - 0.92x_1x_2 - 4.75x_1x_3 + 2.05x_2x_3 \quad (11)$$

The transformed Sauter mean diameter response for T0 and T3 is expressed by the following $\widehat{Y}_3$ and $\widehat{Y}_4$ formulas, respectively:

$$\widehat{Y}_3{}'(\mu\text{m}) = 7.62 - 0.62x_1 - 0.38x_2 + 0.64x_3 - 0.56x_1x_3 \quad (12)$$

$$\widehat{Y}_4{}'(\mu\text{m}) = 7.54 - 0.22x_1 - 0.20x_2 + 0.50x_3 - 0.091{x_2}^2 \cdot 0.66x_1x_2 + 0.06x_1x_3 - 0.27x_2x_3 \quad (13)$$

With: $\widehat{Y}_3{}'^2 = \widehat{Y}_3$ and $\widehat{Y}_4{}'^2 = \widehat{Y}_4$

Polydispersity responses for both examination times are represented respectively to T0 and T3 by the following formulas:

$$\widehat{Y}_5(\%) = 55.68 - 1.94x_1 - 4.87x_2 - 3.50x_3 + 2.89{x_3}^2 - 6.50x_1x_2 - 3.00x_1x_3 + 2.81x_2x_3 \quad (14)$$

$$\widehat{Y}_6(\%) = 71.77 - 7.56x_1 - 8.73x_2 - 3.13x_3 + 2.17{x_3}^2 - 11.06x_1x_2 + 13.63x_1x_3 - 7.92x_2x_3 \quad (15)$$

where x_1, x_2, and x_3 are the linear levels of SA, CA, and CP, respectively; x_1x_2, x_1x_3, and x_2x_3 represent the interaction levels between SA with CA, SA with CP, and CA with CP respectively; and ${x_2}^2$ and ${x_3}^2$ represent the quadratic levels respectively for CA and CP.

The effect of the Independent Variables on Particles Mean Diameter

In terms of individual effects, SA had the most significant contribution in reducing the arithmetical mean diameters ($\widehat{Y}_1$ and $\widehat{Y}_2$) expressed by negative signs in the models; in contrast, CP had a positive coefficient signs for both responses indicating that the increased mean diameters were principally caused by this factor; in the other hand, SA and CP produced the most synergistic interaction effect compared to the other model coefficients and was represented by negative signs, while CA had no clear effect on the arithmetic mean diameter whether it be individual or in interaction.

The evaluation of the third response ($\widehat{Y}_3$) by the response surface plot represented in Fig. 2 showed the factors' effect on Sauter mean diameter ($d_{3,2}$) that was kept in the same order as on the arithmetic mean diameter (d_{m}) in the first examination period for both individuals and interactions, while the high significant effect was seen in the third month aged formulations represented by ($\widehat{Y}_4$) response in terms of interaction between SA and CA that caused considerably the decrease in particles size, and from the linear coefficients, factors respected the same order of effect as in the first examination (T0) time for Sauter mean diameter with difference in the factors impact.

The Effect of the Independent Variables on Polydispersity

Among all the terms of the fifth model ($\widehat{Y}_5$) that had negative signs, both the quadratic coefficient of CA and the interaction between CA and CP have positive signs; similarly, the interaction between SA and CP is presented by a positive sign in the case of the third month analysis (T3) of polydispersity that is represented by the sixth ($\widehat{Y}_6$) model; these interactions are responsible for high polydispersities, while the three independent variables (SA,CA, and CP) have a negative effect on this parameter for the two examination periods with a relatively dominant effect of CA, whereas the real synergistic effect that causes the polydispersities decrease is owing to the interaction between SA and CA in both examination times; this latter interaction showed the same effect on the SMD previously remarked in ($\widehat{Y}_4$) response.

Rheological Results

Modeling the Flow and Thixotropic Parameters

The rheological flow curves displayed a pseudoplastic shear thinning behavior that has been characterized by a logarithmic increase in stress depending on the flow index ($n < 1$) with respect to the applied shear rates, and inversely for the apparent viscosity that decreased continuously when the shear rates increased; these systems presented also a thixotropic behavior illustrated in Fig. 5 and this behavior is required in pharmaceutical and cosmetic semisolid forms [32], and was shown previously in similar mixtures as ternary systems containing fatty alcohols [42], emulsions [8], and SLNs and SLMs [43, 44]; the measure of the area bounded between the up and down curves allowed the quantification of this phenomenon in which the microstructure is disrupted and recovered its shape progressively by applying and removing the shear rates, respectively; this thixotropic behavior indicates that the fluid has a time-dependent property.

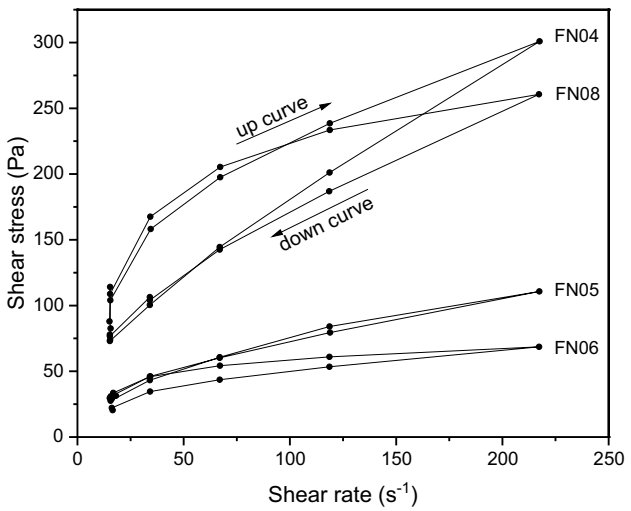


Fig. 5 Two steps hysteresis loop rheograms illustrating the thixotropic behavior for some 3-month aging formulations, and FN05, showing an antithixotropic behavior drawn in the down-curve

The development of rheological models was based on the same strategy conducted with the microscopic models, and three reduced second-order models were built using both flow and thixotropic data, designated respectively for the power law consistency index ($\widehat{Y}_7$), the Casson's yield stress ($\widehat{Y}_8$), and the transformed hysteresis loop area ($\widehat{Y}'_9$), with:

$$\mathrm{Log}_{10}\widehat{Y}_9 = \widehat{Y}'_9,$$

$$\widehat{Y}_7(\mathrm{Pas^n}) = 41.48 + 10.92x_1 + 20.44x_2 + 6.76x_3 - 3.51x_2^2 + 8.06x_1x_2 - 3.05x_1x_3 + 7.38x_2x_3 \quad (16)$$

$$\widehat{Y}_8(\mathrm{Pa}) = 69.30 + 14.75x_1 + 28.91x_2 + 5.79x_3 - 7.63{x_2}^2 + 11.21x_1x_2 - 6.88x_1x_3 + 7.79x_2x_3 \quad (17)$$

$$\widehat{Y}'_9(\mathrm{Pa/s}) = 3.32 + 0.25x_1 + 0.34x_2 - 0.11x_3 - 0.05x_1x_2 + 0.09x_1x_3 + 0.06x_2x_3 \quad (18)$$

where x_1, x_2, and x_3 are the individual levels representing SA, CA, and CP, respectively; x_1x_2, x_1x_3, and x_2x_3 represent the interaction effect between SA with CA, SA with CP, and CA with CP, respectively; and ${x_2}^2$ represents the quadratic coefficient of CA.

The Effect of the Independent Variables on Flow and Thixotropic Behaviors

The consistency and the yield stress are two rheological parameters responsible on the degree of stiffness and viscoelasticity of the structure; they have been similarly affected by the three factors, and CA had the dominant descendent effect followed by SA and CP with less impact; in the other hand, CA and SA have the most significant coefficient in terms of interactions.

The transformed hysteresis area followed the same effect order as the consistency and the yield stress; however, CP is not only less affected, but also causes decrease in the thixotropic index; in contrast, CP interaction had a positive effect either with CA or SA, contrary to CA and SA interaction effect that have influenced negatively the hysteresis area (Fig. 6).

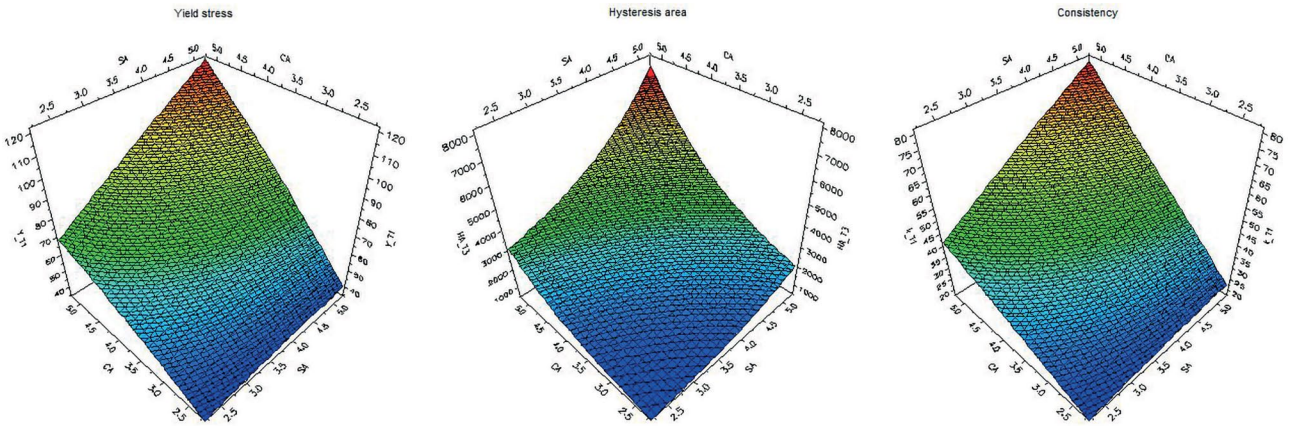


Fig. 6 Response surface plot of factors effect (with centered level of CP of 2.5wt) as function of their resultant responses: from left to right, the yield stress, hysteresis area, and the index of consistency of the power law model

Results of the Transient Shear Experiments and Time-Dependent Rheological Parameters

The modified Weltmann model demonstrated an acceptable fit ($R^2 > 0.98$) to the data obtained from the start-up flow experiments in which a constant shear rate was applied and the monitored stress decays logarithmically over time.

In the majority of the formulations, the stress increased for the first seconds as response to the sudden application of the shear rate (16 s^{-1}) until it hit a maximum value, and then it remains in decrease before reaching a lower plateau, while the second step of shear rate at 119 s^{-1} presented a continuous decrease in the shear stress with different intermolecular breakdown rates.

The data obtained from the first two steps of shear rate did not present as much information as expected; the fit by MLR method gave a lot of insignificant terms unlike the third step that presented more significant coefficients, and thus, it was selected to evaluate the history of structural damage.

Figure 7 represents the stress behavior over time to the induced 385.5 s^{-1} constant shear rate, the stress overshoots firstly as response to higher shear rate, and the plot over the logarithmic scale of time showed almost a straight plateau that took a several seconds before it fastener to decay; regarding these characteristics of viscoelastic and thixotropic fluids, previous studies illustrated the stress overshoot phenomenon in case of polymers solutions [45, 46], and lamellar gel network structures [47].

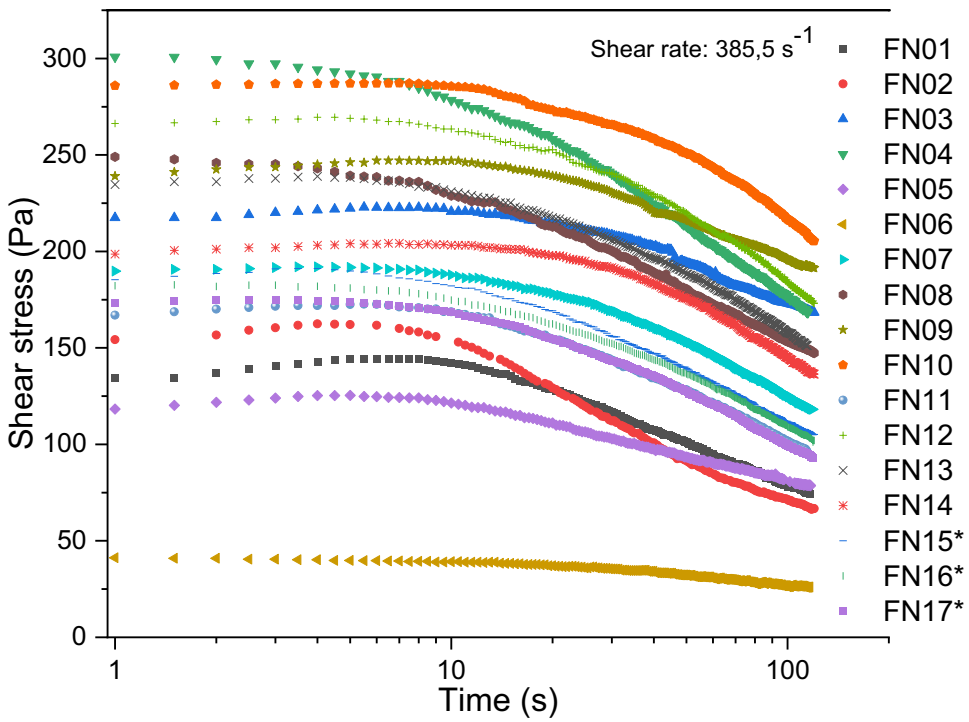


Fig. 7 Thixograms of the formulations at 385.5 s^{-1} constant shear rate (third step)

Modeling Time-Dependent Parameters *A* and *B* by MLR Regression Method

The following two models, whose terms showed the highest significance ($p < 0.01$), are represented by $\widehat{Y}'_{10}$ and $\widehat{Y}'_{11}$ as responses for both transformed (A) and (B), respectively, while their real values can be obtained by retransforming the responses as follow:

$$\widehat{Y}_{10} = 10 \cdot \widehat{Y}'_{10} \text{ and } \widehat{Y}'_{11} = 10 \cdot \widehat{Y}'_{11}$$

This linear transformation aimed to reduce the RSD values.

$$\widehat{Y}'_{10}(\text{Pa}) = 24.93 + 2.11x_1 + 8.24x_2 - 3.16x_3 - 2.93{x_2}^2 + 3.81x_1x_2 - 2.15x_1x_3 \quad (19)$$

$$\widehat{Y}'_{11}(\text{Pa}) = 7.91 + 0.71x_1 + 1.67x_2 - 1.20x_3 - 1.33{x_1}^2 + 1.01x_1x_2 - 1.13x_1x_3 + 0.99x_2x_3 \quad (20)$$

Effect of the Factors on Weltmann *A* and *B* Parameters

Noticeably, the two Weltmann parameters have the same effect (Fig. 8) like the hysteresis area in terms of individual influence of the three factors; however, CP induced a decrease in A and B, while CA caused significantly the increase of the thixotropic parameters compared to SA, but in terms of interactions, these two time-dependent parameters increased as a consequence of SA and CA interaction in opposition with the transformed hysteresis area and in agreement when no transform is applied. However, the transformation of this latter parameter was kept firstly for the reason that more significance is achieved with more significant terms ($p > 0.05$), and secondly the experiments were employed differently.

Evaluation of the Models

The raw data resultant from the microscopic and rheological examinations (see Supplementary File) were evaluated according to the goodness of both R^2 and R^2_{adj}, and satisfactory values of these two parameters with differences that did not exceed 0.02 indicate that the data obtained experimentally are in agreement with the predicted ones.

The efficiency of the prediction for a new combination can be estimated by Q^2; this parameter is related principally by the significance of the used terms in the model as previously explained; in this concern, the lowest values were obtained for the time-dependent models ($\widehat{Y}_{10}$ and $\widehat{Y}_{11}$) representing Weltmann (B) and (A) parameters with 0.892 and 0.914 values, respectively; this may be caused by the stress overshoot which makes difficulties during data fitting even with a good coefficient of correlation that influenced also the model validity which is related to the pure error which itself is related to the reproducibility. The rest of the parameters evaluating the models built in this study are summarized in Table 2.

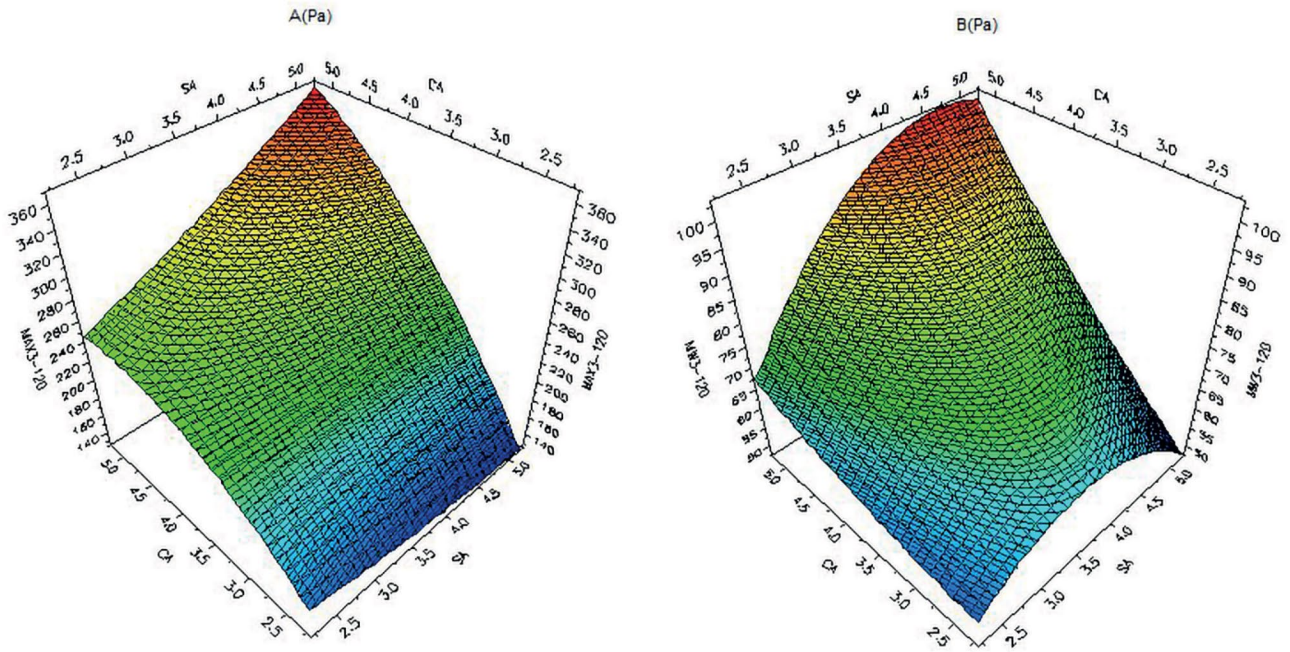


Fig. 8 Response surface plot showing the effect of individual factors with a fixed center level of CP on the parameters: *A* increasing relatively with the factors levels and *B* related to the ratios of the factors

Table 2 Summary list evaluating the developed models

Model	R^2	R^2_{Adj}	Q^2	SDY	RSD	N	M-V	Rep
$\hat{Y}_1$ (μm)	0.989	0.983	0.928	8.15	1.06	17	0.792	0.989
$\hat{Y}_2$ (μm)	0.997	0.995	0.985	5.52	0.40	17	0.826	0.996
$\hat{Y}'_3$ (μm)	0.982	0.976	0.963	0.85	0.13	17	0.969	0.950
$\hat{Y}'_4$ (μm)	0.993	0.987	0.904	0.68	0,08	17	0.831	0.989
$\hat{Y}_5$ (%)	0.987	0.977	0.945	7.58	1.15	17	0.904	0.971
$\hat{Y}_6$ (%)	0.997	0.994	0.983	16,82	1,25	17	0.725	0.997
$\hat{Y}_7$ (Pas^n)	0.995	0.992	0.980	20.58	1,89	17	0.927	0.989
$\hat{Y}_8$ (Pa)	0.987	0.976	0.940	28.45	4.39	17	0.691	0.990
$\hat{Y}'_9$ (Pa/s)	0.994	0.989	0.979	0.35	0.04	17	0.881	0.989
$\hat{Y}'_{10}$ (Pa)	0.973	0.956	0.914	8.10	1.70	17	0.514	0.992
$\hat{Y}'_{11}$ (Pa)	0.981	0.966	0.892	2.27	0,42	17	0.529	0.993

$\hat{Y}_1$ T0_*d*m(μm), $\hat{Y}_2$ T3_*d*m(μm), $\hat{Y}'_3$ T0_$d_{3,2}$(μm), $\hat{Y}'_4$ T3_$d_{3,2}$ (μm), $\hat{Y}_5$ T0_ *D*(%), $\hat{Y}_6$:T3_ *D*(%), $\hat{Y}_7$ *K*(Pas^n), $\hat{Y}_{8\tau_0}$(Pa), $\hat{Y}'_9$ hysteresis area (Pa/s), $\hat{Y}'_{10}$ *A* (Pa), $\hat{Y}'_{11}$ *B* (Pa)

SDY standard deviation, *M-V* model validity, *Rep* reproducibility

() transformed function

Discussion

The solid lipid microparticles in this study are formulated by the simple hot emulsification method; two mixtures are separately prepared where one contained only a warmed amount of water and the other contained molten lipid and surfactant mixture; in this latter mixture, the hydrocarbon chains are dissociated which involve formation of mobile liquid crystals due to the interaction between the solid lipids and Tween 80. After the high shear homogenization step, the formulation is left to cool down, at room temperature; a viscoelastic gel network is formed initially with a lower rigidity than after succession of time; during this period, the fatty amphiphiles are self-assembled into a gel network; this was noticed when the formulation is transformed from a liquid-like flow to a semisolid form; this transformation can be explained by the solubilization of the polyoxyethylene chains in the nonionic surfactant molecules [41].

The optical photomicrographs showed different shapes of lipid particles embedded within a gel network in the bulk water phase; furthermore, this crystalline gel network swells with time and the difference can be seen comparatively between T0 and T3 analysis; meanwhile, the hydrophilic and hydrophobic bounds are gathered due to the interaction between the amphiphilic bilayers and water in the presence of the surfactant [48]; in this study, the swelling potency was higher at high amounts (e.g., FN08) but not in all situations (e.g., FN01 > FN03); thus, the swelling was influenced principally by the total amount of fatty amphiphiles and then their ratio at low amounts; this was illustrated by the Sauter mean diameter and polydispersity both on the third month analysis accordingly with the structure breakdown parameter (*B*), and from the response surface plots; it formed some specific undesirable (FA) ratios presenting unsuitable results deteriorating as follow: (SA:CA)/(2.2:2.2) > (5.2:2.2) > (2.2:2.2); these results are in agreement with those obtained by Barry and Eccleston [41] in which the strengthening of the gel network formed with the homologous cetostearyl alcohol was higher than with pure cetyl or stearyl alcohols in the system; in the same study, it was found also that ternary systems and emulsion consistencies went higher when high amounts of mixed emulsifiers were employed, which agree with the results found with the studied SLMs in this work, and was shown in all rheological parameters when FA and CP amount was set at high levels; moreover, the chain length played a principal role on determination of the influence of each constituent; the consistency, yield stress, and thixotropic parameters increased inversely with chain length; compared with the microscopic parameters, this influence was in accordance only in the case of CP (C32) that participated on SLM destabilization contrary to fatty alcohols that contributed to decrease the particle size inversely with the rheological order, showing SA (C18) influencing more than CA (C16); this comparison was based on the individual effect only, but when comparing the response surface plots that took in the influence of all the terms, the relationship between the rheological and microscopic data went evident when comparing the third month polydispersities, SMD mean diameter, and the structure breakdown (*B*) parameters, but statistically, the most influence in the majority of the parameters was shown in terms of interaction

between SA and CA; thus, the interactions between components must be optimized to better select the most influencing ratio leading to relatively durable stabilization.

Optimal Ratio (OR)

In this step, the study was conducted to optimize the ratio of the three factors; thus, the optimizer tool presented by the software was used to select the best composition of lipids that could provide the best combinations to stabilize the SLMs for the longest possible time, and for that purpose, all the significant and non-significant terms of the models were put in the process; however, the transformations were kept, the rheological parameters were maximized, and the microscopic parameters were minimized for both examination times.

When the optimization is based only on the rheological data, the ratio would be equivalent to the following amounts: 5.2:5.2:2.2373, while the combination of 5.2:5.2:2.3053 is obtained when only the microscopic data are used, and when all data are used in the optimization process, the optimal ratio among eight propositions was found to be 5.2:5.2:2.2698 (SA:CA:CP), equivalent to the weight fraction of 0.41:0.41:0.18, which illustrates the strength relationship between particle size and polydispersity with the rheological parameters.

It was remarkable and must be presented that the fatty alcohols ratio constantly was predicted for SA:CA (1:1), which is consistent with the results obtained previously [21] in which the ratio was optimized using molecular dynamics simulation, and the formation mechanism of the complex gel network is well explained.

Validation of the Optimized Formulation (OF)

In order for the results of the models to be valid, the optimized ratio has been used to prepare the optimal formulation (OF), while making sure to work in the same conditions as with the seventeen formulations conducted these results; in addition, the same batches of raw material were reused once again, and as results of the (OF), none of the experimental results exceeded 10% error from the predicted values; that the maximal error was shown for the consistency index with 8.57% from the predicted values, this is reasonable since the standard deviation of this response showed relatively high value, while the minimum percent error was shown for the result of (T0) arithmetic mean diameter with only 0.31% from the predicted value; all results of the optimized formulation are summarized in Table 3.

TBH-Loaded SLMs Results

The three TBH-loaded SLMs have a similar appearance to the un-loaded formulations with the slowest (3–7 days) transformation to the semisolid form was observed for the 6% lipid preparation (TBH-SLM-6) that presented a liquid-like flow which lasted more than 2 days, and after 1 week, all the formulations are semisolids, indicating development of a lamellar gel network structure with more swelling capacity for high lipids content formulations.

The microscopic models at T0 predicted arithmetical mean diameters around 32 µm for the three formulations (un-loaded formulations of 6%, 9%, and 12% lipids), which was revealed similarly in previous studies [16, 49] investigating the influence of particle size as function of lipids concentrations that no significant change in the particles size can occur due to the increased amount of a specified lipid combination; thus, the influence of the ratio in this study can be confirmed dominant against the total amount of lipids in controlling this parameter. However, the macroscopical unentrapped drug particles were apparent before gelation of the formulation; accordingly, in the TBH-SLM-6, the mean diameter was found to be 47.61 µm with an error of 31.72% to the predicted value; the polydispersity (89.42%) of the particles was probably the cause with 29.98% higher value than the predicted one (see Table 4 in the supplementary file); furthermore, the additional factor (API) influenced models' responses and was the main cause for this heterogeneity. The mean diameters and polydispersities results of the other two formulations (TBH-SLM-9 and TBH-SLM-12) were closely predicted by the models with less than 15% error.

The flow curves of the three terbinafine-HCl-loaded SLMs showed a pseudoplastic shear thinning behavior. The rheological parameters were all altered by the addition of drug particles; the low consistency index of the formulations (TBH-SLM-9 and TBH-SLM-12) did not reach the predicted values ($\hat{Y}_7$) similarly for the yield stress parameter ($\hat{Y}_8$) with errors that can exceed 20%.

The formulations presented an anti-thixotropic behavior (negative hysteresis area) that is related to structural rearrangement and particle aggregation under the effect of the applied shear deformation; this significant change in behavior does not refer to instabilities [50] but limited the prediction of the rheological models built based on the core lipids, whereas the gel network structure continued to develop over time as revealed in Fig. 9 which implies more structural stability of the formulations even in the presence of drug molecules.

In Vitro Drug Release and Permeation Results

In addition to being less consistent and presenting visual particles, the TBH-SLM-6 exhibited low drug percentage of 90.3%, and in contrast, the 9% and 12% lipids formulations showed more than 98% of terbinafine-HCl entrapped and therefore the high lipid content formulations were selected

Table 3 Results of the optimized formulation and the percent error between the predicted and observed values

Model	$\hat{Y}_1$ (µm)	$\hat{Y}_2$ (µm)	$\hat{Y}'_3$ (µm)	$\hat{Y}'_4$ (µm)	$\hat{Y}_5$ (%)	$\hat{Y}_6$ (%)	$\hat{Y}_7$ (Pas^n)	$\hat{Y}_8$ (Pa)	$\hat{Y}'_9$ (Pa/s)	$\hat{Y}'_{10}$ (Pa)	$\hat{Y}'_{11}$ (Pa)
Predicted values	32.1	28.1	44.3	39.1	43.7	43.8	78.2	120.2	7706.4	374.3	104.2
Observed values ± SD	32.2 ± 0.65	27.8 ± 0.48	44.5 ± 0.71	39.9 ± 0.64	45.8 ± 0.71	45.9 ± 0.56	71.5 ± 0.90	118.8 ± 1.19	7545.6 ± 181.1	367.8 ± 3.77	96.8 ± 0.29
Error (%)	0.31	1.07	0.46	2.05	4.81	4.79	8.57	1.16	2.09	1.74	7.10

Essays ($n = 3$) for the rheological parameters, ($n \sim 400$) of particles

Table 4 Drug content and pharmacokinetics of the terbinafine-HCL-loaded formulations

Formulation	TBH-SLM-6	TBH-SLM-9	TBH-SLM-12
Drug content (%)	90.3 ± 1.6	98.2 ± 0.4	98.9 ± 0.7
Higuchi constant (K_H)	NA	29.20 ± 1.61	17.03 ± 1.38
Release rate (µg/*h*)	NA	2615.3	1613.0
Permeation (µg/cm^2 /*h*)	NA	670.6	413.6

NA not applied

Essays ($n = 3$)

to be considered for the drug release and permeation comparison study.

The pharmacokinetic tests presented in Fig. 10 are representatives for a sustained drug delivery profile with an initial (1 h) "burst" release effect of about 32.9% for the TBH-SLM-9 against 0.06% for the TBH-SLM-12; the low lipid content formulation released more drug of 87.6% up to 12 h and 51.1% was the total drug released for the highest lipid content formulation with release rates, respectively, to 2.6 and 1.6 mg/h. The TBH-SLM-12 has more uniformly entrapped the drug while the TBH-SLM-9 can enhance the drug penetration into the skin; however, the two discussed characteristics are recommended for topical dosage forms [51]. The results of these tests are summarized in Table 4.

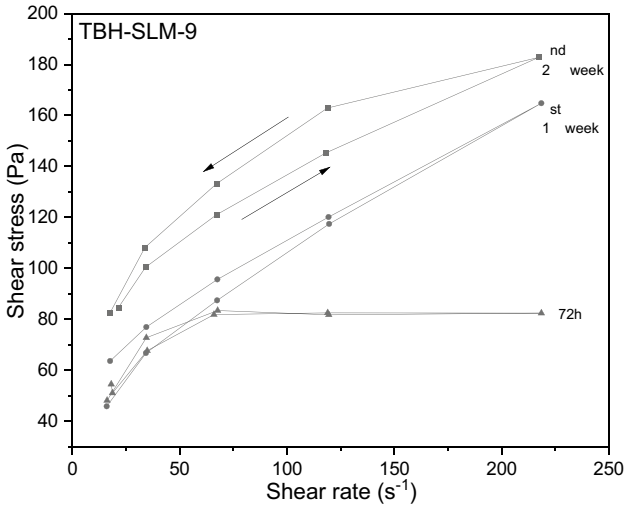


Fig. 9 Rheograms of TBH-SLM-9 formulation showing an anti-thixotropic behavior over 2 weeks of structural development

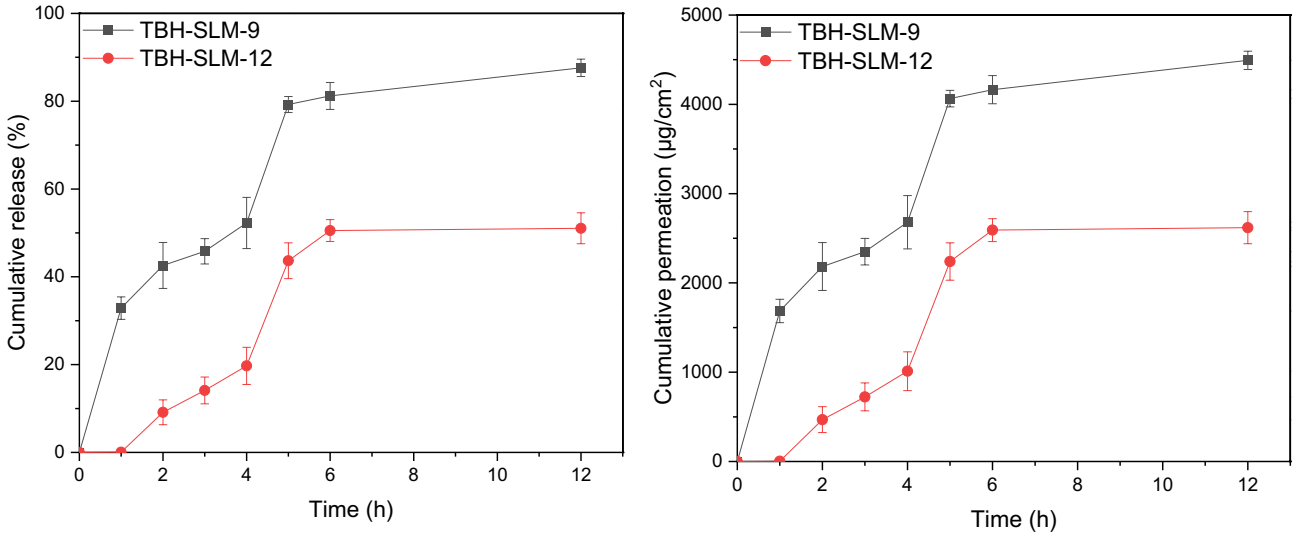


Fig. 10 Comparative between two terbinafine-HCl-loaded SLMs (TBH-SLM-9 and TBH-SLM-12) showing a sustained release profile

Conclusion

In summary, this study examined solid lipid microparticles that have been successfully produced in the absence of an oil phase by high shear homogenization and hot emulsification methods; these complex systems revealed different structural and rheological behaviors with a strong relationship in-between and relative dependency on the lamellar gel network and its swelling capacity that is developed and strengthen over time. The following points highlight the most important findings in this study:

1. Eleven regression models were built in order to evaluate and predict the structural and rheological behaviors of SLMs composed of stearyl alcohol, cetyl alcohol, and cetyl palmitate in the presence of a nonionic surfactant.
2. These models meant to organize the employment of the studied fatty amphiphiles in the cosmetic and pharmaceutical semisolid formulations.
3. RSM conducted successfully the optimization of these lipids leading to a ratio of SA:CA:CP (0.41:0.41:0.18) as an optimal blending formulation that did not showed a significant difference in particle size and polydispersities during the storage time, which may refer to a shorter structural rearrangement time and could prevent particle aggregation and ensure a consistent structure and longer-term stability.
4. The optimized formulation presented a shear thinning and thixotropic behaviors with rheological and microscopic parameters approachable to the predicted values with an error that did not exceed 10% in tests parameters.
5. Terbinafine-HCl (API) was used to verify the findings of this study (see the supplementary file); the developed mathematical models have no absolute applicability in the presence of an additional factor, and however, the gel network is continuously developed in the semisolid dosage SLMs which can lead to more stabilized structures.
6. Terbinafine-HCl-loaded SLMs were formulated using the optimized ratio of lipids at three levels (6%, 9%, and 12%); the more lipid content existed in the formulation, the more drug content is uniformly higher and more drug release profile is sustained.

Supplementary Information The online version contains supplementary material available at https://doi.org/10.1007/s12247-022-09642-0.

Acknowledgements We would like to thank SAIDAL of Medea for providing facilities in conducting this study.

Declarations

Conflict of interest No potential conflict of interest was reported by the authors and we have participated in: Conception, design, analysis and interpretation of the data, Revising the article critically, Approval of the final version. This manuscript has not been submitted to, nor is under review at, another journal or other publishing venue.

References

1. Eccleston GM. Functions of mixed emulsifiers and emulsifying waxes in dermatological lotions and creams. Colloids Surfaces A Physicochem Eng Asp. 1997;123–124:169–82.

2. Barry BW, Saunders GM. Kinetics of structure build-up in self bodied emulsions stabilized by mixed emulsifiers. J Colloid Interface Sci. 1972;41:331–42.
3. Cunningham GE, Alberini F, Simmons MJH, O'sullivan JJ. Understanding the effects of processing conditions on the formation of lamellar gel networks using a rheological approach. Chem Eng Sci Elsevier. 2021;242:116752.
4. Gibson M. Pharmaceutical preformulation and formulation. Drugs Pharm Sci. 2001;199:199.
5. Vu HD, Tran HH, Cong CP, Nguyen HMT, Nguyen TT. Investigating molecular mechanism for the stability of ternary systems containing cetrimide, fatty alcohol and water by using computer simulation. J Mol Graph Model Elsevier. 2020;95:107500.
6. Djuris J, Vasiljevic D, Jokic S, Ibric S. Application of D-optimal experimental design method to optimize the formulation of O/W cosmetic emulsions. Int J Cosmet Sci Wiley Online Library. 2014;36:79–87.
7. Barry BW. The self bodying action of the mixed emulsifier sodium dodecyl sulfate/cetyl alcohol. J Colloid Interface Sci Elsevier. 1968;28:82–91.
8. Barry BW, Saunders GM. The self-bodying action of alkyltrimethylammonium bromides/cetostearyl alcohol mixed emulsifiers; Influence of quaternary chain length. J Colloid Interface Sci. 1971;35:689–705.
9. Eccleston GM, Behan-Martin MK, Jones GR, Towns-Andrews E. Synchrotron X-ray investigations into the lamellar gel phase formed in pharmaceutical creams prepared with cetrimide and fatty alcohols. Int J Pharm Elsevier. 2000;203:127–39.
10. Jaspart S, Piel G, Delattre L. Evrard B is equivalent to SLNs. 2005;2:75–87.
11. Sznitowska M, Wolska E, Baranska H, Cal K, Pietkiewicz J. The effect of a lipid composition and a surfactant on the characteristics of the solid lipid microspheres and nanospheres (SLM and SLN). Eur J Pharm Biopharm [Internet]. Elsevier B.V.; 2017;110:24–30. Available from: https://doi.org/10.1016/j.ejpb.2016.10.023.
12. Jaspart S, Piel G, Delattre L, Evrard B. Solid lipid microparticles: formulation, preparation, characterisation, drug release and applications. Expert Opin Drug Deliv Taylor & Francis. 2005;2:75–87.
13. Wolska E, Sznitowska M, Chorążewicz J, Szerkus O, Radwańska A, Markuszewski MJ, et al. Ocular irritation and cyclosporine A distribution in the eye tissues after administration of Solid Lipid Microparticles in the rabbit model. Eur J Pharm Sci Elsevier. 2018;121:95–105.
14. Sainaga Jyothi VGS, Ghouse SM, Khatri DK, Nanduri S, Singh SB, Madan J. Lipid nanoparticles in topical dermal drug delivery: does chemistry of lipid persuade skin penetration?. J Drug Deliv Sci Technol [Internet]. 2022;69:103176. Available from: https://www.sciencedirect.com/science/article/pii/S1773224722000855.
15. Seetapan N, Bejrapha P, Srinuanchai W, Puttipipatkhachorn S, Ruktanonchai U. Nondestructive rheological measurement of aqueous dispersions of solid lipid nanoparticles: effects of lipid types and concentrations on dispersion consistency. Drug Dev Ind Pharm Taylor & Francis. 2010;36:1005–15.
16. Lippacher A, Müller RH, Mäder K. Preparation of semisolid drug carriers for topical application based on solid lipid nanoparticles. Int J Pharm Elsevier. 2001;214:9–12.
17. Grewal IK. Application of central composite design for development and optimization of eflornithine hydrochloride-loaded sustained release solid lipid microparticles. 2022;12:618–37.
18. Pena L, Lee B, Stearns J. Secondary structural rheology of a model cream. J Soc Cosmet Chem. 1994;45:77–84.
19. Tan ML, Choong PFM, Dass CR. Recent developments in liposomes, microparticles and nanoparticles for protein and peptide drug delivery. Peptides Elsevier. 2010;31:184–93.
20. Umeyor CE, Kenechukwu FC, Uronnachi EM, Osonwa UE, Nwakile CD. Solid lipid microparticles (SLMs): an effective lipid based technology for controlled drug delivery. Am J PharmTech Res. 2012;2:1–18.
21. Hoang VD, Cong CP, Tran HH, Nguyen HMT, Nguyen TT. Influence of fatty alcohol mixing ratios on physicochemical properties of stearyl–cetyl–polysorbate 60–water ternary system: Insights from experiments and computer simulations. Colloid Polym Sci [Internet]. 2021;299:1885–900. Available from: https://doi.org/10.1007/s00396-021-04874-x.
22. Sinha P, Srivastava N, Rai VK, Mishra R, Ajayakumar PV, Yadav NP. A novel approach for dermal controlled release of salicylic acid for improved anti-inflammatory action: Combination of hydrophilic-lipophilic balance and response surface methodology. J Drug Deliv Sci Technol Elsevier. 2019;52:870–84.
23. Gorantla S, Saha RN, Singhvi G. Exploring the affluent potential of glyceryl mono oleate–myristol liquid crystal nanoparticles mediated localized topical delivery of Tofacitinib: Study of systematic QbD, skin deposition and dermal pharmacokinetics assessment. J Mol Liq Elsevier. 2022;346:117053.
24. Shinde G, Sonchhatra A, Shelke S, Pathan I. Design, optimization and in-vivo characterization of mupirocin loaded nanostructured lipid carrier based gel for effective treatment of impetigo. J Drug Deliv Sci Technol Elsevier. 2022;67:102872.
25. Esnaashari SS, Amani A. Optimization of noscapine-loaded mPEG-PLGA nanoparticles and release study: a response surface methodology approach. J Pharm Innov Springer. 2018;13:237–46.
26. Lebouachera SEI, Ghriga MA, Salha G Ben, Hadri H El, Hasanzadeh M, Drouiche N, et al. Optimization of zero-shear viscosity for HPAM-Polystyrene microspheres formulations through experimental design approach. J Polym Res [Internet]. Springer Netherlands; 2021;28. Available from: https://doi.org/10.1007/s10965-021-02473-6.
27. Shah S, Bhanderi B, Soniwala M, Chavda J. Lutein-Loaded solid lipid nanoparticles for ocular delivery: Statistical optimization and ex vivo evaluation. J Pharm Innov. Springer; 2021;1–15.
28. Salager JL. Emulsion properties and related know-how to attain them, en Pharmaceutical emulsions and suspensions. In: Nielloud F, Marti-Mestres G, editors. Drugs and pharmaceutical science series vol. 105, Chap. 3. Marcel Dekker, New York; 2000.
29. Bonn D, Denn MM, Berthier L, Divoux T, Manneville S. Yield stress materials in soft condensed matter. Rev Mod Phys. 2017;89:1–44.
30. Razavi A, Shirani E, Sadeghi MR. Numerical simulation of blood pulsatile flow in a stenosed carotid artery using different rheological models. J Biomech [Internet]. Elsevier; 2011;44:2021–30. Available from: https://doi.org/10.1016/j.jbiomech.2011.04.023.
31. Weltmann RN. Breakdown of thixotropic structure as function of time. J Appl Phys. 1943;14:343–50.
32. Rawat A, Gupta SS, Kalluri H, Lowenborg M, Bhatia K, Warner K. Rheological characterization in the development of topical drug products. Role Microstruct Top Drug Prod Dev. Springer; 2019. p. 3–45.
33. Elmataeeshy ME, Sokar MS, Bahey-El-Din M, Shaker DS. Enhanced transdermal permeability of Terbinafine through novel nanoemulgel formulation; development, in vitro and in vivo characterization. Futur J Pharm Sci Elsevier. 2018;4:18–28.
34. Müller-Goymann CC. Preparation, characterization, and in vitro permeation study of terbinafine HCl in poloxamer 407-based thermogelling formulation for topical application. AAPS PharmSciTech Springer. 2011;12:496–506.
35. Ameeduzzafar, Qumber M, Alruwaili NK, Bukhari SNA, Alharbi KS, Imam SS, et al. BBD-based development of itraconazole loaded nanostructured lipid carrier for topical delivery: in vitro evaluation and antimicrobial assessment. J Pharm Innov [Internet]. 2021;16:85–98. Available from: https://doi.org/10.1007/s12247-019-09420-5.
36. Sareen R, Bhardwaj V, Mehta V, Sharma A. Topical gel incorporated with non-ionic surfactant based solid lipid microspheres of ketoprofen: physicochemical analysis and anti-inflammatory evaluation. Int J Pharm Pharm Sci. 2015;7:200–6.

37. Rowe RC, Sheskey P, Quinn M. Handbook of pharmaceutical excipients. Libros Digitales-Pharmaceutical Press; 2009.
38. Moore J. Final report on the safety assessment of octyl palmitate, cetyl palmitate and isopropyl palmitate. J Am Coll Toxicol. 1982;1:13–35.
39. Williams SO, Long S, Allen J, Wells ML. Scale-up of an oil/water cream containing 40% diethylene glycol monoethy ether. Drug Dev Ind Pharm Taylor & Francis. 2000;26:71–7.
40. Barreiro-Iglesias R, Alvarez-Lorenzo C, Concheiro A. Poly(acrylic acid) microgels (carbopol® 934)/surfactant interactions in aqueous media: Part I: Nonionic surfactants. Int J Pharm [Internet]. 2003;258:165–77. Available from: https://www.sciencedirect.com/science/article/pii/S0378517303001819.
41. Barry BW, Eccleston GM. Influence of gel networks in controlling consistency of o/w emulsions stabilised by mixed emulsifiers. J Texture Stud Wiley Online Library. 1973;4:53–81.
42. Eccleston GM. The influence of fatty alcohols on the structure and stability of creams prepared with polyethylene glycol 1000 monostearate/fatty alcohols. Int J Cosmet Sci. 1982;4:133–42.
43. Lukic M, Pantelic I, Daniels R, Müller-Goymann C, Savic M, Savic S. Moisturizing emulsion systems based on the novel long-chain alkyl polyglucoside emulsifier: the contribution of thermo-analytical methods to the formulation development. J Therm Anal Calorim. 2013;111:2045–57.
44. Lauterbach A, Müller-Goymann CC. Comparison of rheological properties, follicular penetration, drug release, and permeation behavior of a novel topical drug delivery system and a conventional cream. Eur J Pharm Biopharm [Internet]. Elsevier B.V.; 2014;88:614–24. Available from: https://doi.org/10.1016/j.ejpb.2014.10.001.
45. Osaki K, Inoue T, Uematsu T. Stress overshoot of polymer solutions at high rates of shear: semidilute polystyrene solutions with and without chain entanglement. J Polym Sci Part B Polym Phys Wiley Online Library. 2000;38:3271–6.
46. Richardson RK, Ross-Murphy SB. Non-linear viscoelasticity of polysaccharide solutions. 1: Guar galactomannan solutions. Int J Biol Macromol. 1987;9:250–6 Elsevier.
47. Datta A, Tanmay VS, Tan GX, Reynolds GW, Jamadagni SN, Larson RG. Characterizing the rheology, slip, and velocity profiles of lamellar gel networks. J Rheol N Y N Y Trans Soc Rheol. 2020;64:851–62.
48. Davies AR, Amin S. Microstructure design of CTAC:FA and BTAC:FA lamellar gels for optimized rheological performance utilizing automated formulation platform. Int J Cosmet Sci. 2020;42:259–69.
49. El-Kamel AH, Al-Fagih IM, Alsarra IA. Testosterone solid lipid microparticles for transdermal drug delivery Formulation and physicochemical characterization. J Microencapsul. 2007;24:457–75. Taylor & Francis.
50. Gianeti MD, Gaspar LR, Bueno de Camargo Júnior F, Berardo Gonçalves Maia Campos PM. Benefits of combinations of vitamin A, C and E derivatives in the stability of cosmetic formulations. Mol. 2012.
51. Motawea A, Borg T, Abd El-Gawad AE-GH. Topical phenytoin nanostructured lipid carriers: design and development. Drug Dev Ind Pharm. 2018;44:144–57. Taylor & Francis.

Publisher's Note Springer Nature remains neutral with regard to jurisdictional claims in published maps and institutional affiliations.